HIGH-RESOLUTION CENTIMETER RADIO CONTINUUM AND AMMONIA MASER OBSERVATIONS OF THE W51 REGION OF STAR FORMATION

R. A. GAUME AND K. J. JOHNSTON
Center for Advanced Space Sensing, Code 7200, Naval Research Laboratory, Washington, DC 20375-5351

AND

T. L. WILSON
Max-Planck-Institut für Radioastronomie, Auf dem Hügel 69, 53 Bonn 1, Germany

ABSTRACT

High angular resolution and high-sensitivity observations at wavelengths of 1.3 and 3.6 cm have detected three new ultracompact emission regions in the core of the W51 (regions d and e). In total, five ultracompact continuum objects of diameter less than 300 to 3000 AU are located in W51 d and e. These sources may best be explained as photoionized stellar winds. This suggests that there may exist a quasi-stable point in early stellar evolution where observable H II regions are formed by stellar winds around massive stars.

These observations demonstrate that the taxonomy of H II region classification may be heavily affected by sensitivity, and a lack of complete spatial sampling by interferometric mapping. For example, the W51 d region, previously classified as cometary, is shown by our higher resolution and sensitivity observations also to have the properties normally associated with shell-like regions. These new observations suggest that the bow shock model, which is suggested to explain the morphology of cometary H II regions, but cannot explain shell sources, does not fully explain the W51 d H II region.

The $J, K = (9, 8)$ NH_3 maser associated with W51 d has been shown to have a minimum brightness temperature of 2.7×10^6 K. This maser is most probably saturated.

Subject headings: H II regions — ISM: individual (W51) — ISM: molecules — ISM: structure — masers — radio continuum: interstellar

1. INTRODUCTION

W51 is a region of on-going star formation in the constellation Aquila. At a distance of about 7 kpc ($1''$ is 0.03 pc) the W51 complex has been studied by numerous investigators. The centimeter continuum emission from the W51 region was shown by Martin (1972) to consist of eight distinct components, W51 a–h. The strongest of the eight components, W51 e, and nearby W51 d were studied by Scott (1978) who found two compact continuum components, W51 e_1 and e_2, in addition to the larger H II regions. OH and H_2O masers, which trace active regions within star-forming complexes, have been found toward the W51 d and e regions (Gaume & Mutel 1987; Schneps et al. 1981; Genzel et al. 1981). Some of the clusters of OH and H_2O masers are closely associated with radio continuum components. Others are found in regions without detected continuum sources. Studies of thermal emission from molecules such as NH_3 (Rudolph et al. 1990; Mauersberger, Henkel, & Wilson 1987; Ho, Genzel, & Das 1983) have traced warm, dense regions within W51 d and W51 e.

Madden et al. (1986) found the first intense NH_3 maser emission in the $(J, K) = (9, 6)$ inversion line. Monitoring of the (9, 6) line in W51 by Wilson & Henkel (1988) and Wilson, Johnston, & Henkel (1990) showed time variability on a period of less than 1 year. In 1986 the most intense (9, 6) maser line was located near W51 d, but after 1987 July, this maser became a factor of 10 weaker, and the intensities of the (9, 6) maser features in the general vicinity of W51 e_1 and e_2, ~40'' SW of W51-IRS 2, increased by more than a factor of 10. Very long baseline interferometry observations (Pratap et al. 1991) have shown that the (9, 6) line emission arises in W51 e from regions

of less than 0.1 mas in size, in two areas NE of W51 e_1, and NW of W51 e_2.

The (9, 6) NH_3 maser arises from ortho-NH_3. Mauersberger et al. (1987) detected other NH_3 maser lines from para-NH_3. Confirmation that the NH_3 emission toward W51 d in the (9, 8) para transition could be attributed to the maser process was provided by Wilson et al. (1990), placing a lower limit on the brightness temperature of the emission at 1600 K. Wilson, Gaume, & Johnston (1991) were able to set a lower limit to the brightness temperature of this (9, 8) maser of ≥ 260,000 K and found the NH_3 maser projected onto a previously undetected ultracompact H II region. To limit the brightness temperature of the (9, 8) NH_3 maser yet further and to investigate the continuum emission in the W51 d and e regions we have employed the VLA[1] in its highest resolution A array.

2. OBSERVATIONS

The observations occurred on 1991 July 20 in both spectral line and continuum modes of the VLA. All available antennas were used in the A-array, which provides baseline lengths from 0.7 to 36 km. The source 3C 286 was used as the primary flux density calibrator for the observations (assumed flux density, 5.3 and 2.4 Jy at 3.6 and 1.3 cm, respectively), and 3C 84 as a bandpass calibrator for the spectral line observations (derived flux density 30.8 Jy at 1.3 cm). The phase calibrator was 1923 + 210 (derived flux density 1.49 and 1.46 Jy at 3.6 and 1.3

---

[1] The VLA is a telescope of the National Radio Astronomy Observatory (NRAO) which is operated by Associated Universities, Inc., under cooperative agreement with the National Science Foundation.

cm, respectively). The data were calibrated and reduced using the AIPS software package of the NRAO as implemented on NRL computer systems.

Observations of W51 were conducted in continuum mode using the 3.6 cm receiver system. The 3.6 cm observations used a central pointing position of $\alpha(1950) = 19^h21^m24^s.186$ $\delta(1950) = 14°24'55".5$. The 3.6 cm observations employed dual 50 MHz IF channels and consisted of three scans of 15 minutes duration. To improve coverage of the transform plane each scan was separated by 2 hr. The u, v data were edited and transformed into 1024 × 1024 pixel images (pixel size = 0".07). All images were "cleaned" with a beam deconvolution algorithm. The FWHM resolution of the images is 0".21 × 0".20 (uniform weighting). Because of good phase stability at 3.6 cm during the observations, self-calibration did not improve the overall quality of the data. Primary beam attenuation was not a significant factor, and no correction was applied to the 3.6 cm data.

The line mode observations, conducted with the 1.3 cm receiver system, also used dual IF channels and consisted of 21 scans on-source, of each of ∼10 minutes duration. The central pointing position for the 1.3 cm observations was $\alpha(1950) = 19^h21^m22^s.166$ $\delta(1950) = 14°25'11".9$. The 1.3 cm observations covered an hour angle range of about 6 hours. The first IF channel was 0.781 MHz wide and was separated into 128 spectral line channels. Channel 0 of the 128 line channels was a wide-band channel 0.586 MHz wide. The remaining 127 Hanning weighted narrow channels had a width of 6.104 kHz (0.077 km s^{-1}). Channel 64 of the 127 narrow channels was tuned to the frequency of the NH$_3$ (9, 8) inversion transition, 23,657.471 MHz, at an LSR velocity of 55.4 km s^{-1}. The peak flux density was found in channel 66. The antenna gain solutions were improved through a self-calibration algorithm operating on the channel 66 data. The improved antenna gains were applied to the entire spectral line database. The self-calibration scheme modified the fitted position of the feature in channel 66 by less than 1/10 beamwidth (FWHM). No subsequent correction was made for this effect. The data for all channels were edited and transformed into 256 × 256 pixel images (pixel size = 0".024). A mean continuum image was constructed from a total of 86 off-line narrow channels taken from both ends of the bandpass. This continuum image was subtracted in the image plane from all channel images. Beam sidelobes were removed from the resulting "line only" image cube using a beam deconvolution algorithm. The resolution of the restored images was 0".074 × 0".072 (uniform weighting). Primary beam attenuation was not a factor for the 1.3 cm NH$_3$ maser observations, and no correction was made in the data.

The second 1.3 cm IF channel was 25 MHz wide and was separated into eight spectral line channels. The first channel (channel 0) of the eight line channels was a wide-band channel 18.750 MHz wide averaged over the inner 75% of the 25 MHz band. The remaining seven Hanning weighted narrow channels each had a width of 3.125 MHz. The center channel (channel 4) of the seven narrow channels was tuned to a region without line emission, 13 MHz lower than the central frequency of the first 1.3 cm IF channel. As the purpose of the second IF channel was to produce a high-resolution image of the W51 1.3 cm continuum emission, further data processing was performed only on the channel 0 wide-band data base. A highly tapered, lower resolution image was made from the 1.3 cm wide-band data to identify emission features. The 1.3 cm emission was found localized in three regions which were sub-

sequently imaged and simultaneously cleaned in three separate fields using image sizes of up to 1024 × 1024 pixels of size 0".024. A self-calibration algorithm was applied to the channel 0 data. The self-calibration scheme modified the fitted position of features in the image by less than 1/20 beamwidth. No correction has been made for this effect. The FWHM resolutions of the restored 1.3 cm images are 0".075 × 0".073 (uniform weighting) and 0".094 × 0".093 (natural weighting). Primary beam attenuation is a significant factor in the 1.3 cm wide field continuum images. A correction for this attenuation has been applied to the data in the image plane.

3. RESULTS

A contour plot of the 2 cm continuum from the W51 region is shown in Figure 1a (from Gaume & Mutel 1987). A contour plot of our 3.6 cm image is shown in Figure 1b. The striking differences between Figures 1a and 1b are easily explained as resulting from differing observational parameters, namely spatial resolution and sensitivity. Although 3.6 cm data have a sensitivity about 25 times greater than that of the 2 cm data and a resolution almost 5 times greater, the 3.6 cm data are not sensitive to continuum emission with a scale larger than about 5", whereas the 2 cm data in Figure 1a are sensitive to scale sizes of up to about 20". The result is that extended emission, easily seen in the 2 cm data, is not well represented in the 3.6 cm data. A directly related problem for the 3.6 cm data are the errors that are introduced in the image plane because of inadequate short-spacing u, v coverage of the strong extended emission. These errors cause large-scale undulations, both positive and negative, in the background noise level (see Perley 1989). The best solution to this problem is to obtain better short-spacing coverage. However, the errors can be minimized, to a certain extent, by editing out the very short, undersampled spacings in the coverage, which introduce the most significant errors.

The radio continuum emission in the core of the W51 d and e regions is found in three locations shown in Figure 1: W51 d, W51 e, and W51 e$_1$/e$_2$. Figure 2a is a contour plot of the 3.6 cm emission toward the W51 d region with a resolution of 0".21. Small crosses mark the positions of H$_2$O masers (Schneps et al. 1981), triangles the positions of OH masers (Gaume & Mutel 1987), a large cross the position of $(J, K) = (9, 8)$ NH$_3$ masers, and broken contours the $(J, K) = (3, 3)$ NH$_3$ thermal emission (Ho et al. 1983). Two of the continuum regions seen in Figure 2a were identified by Wood & Churchwell (1989). The strongest, arclike component in Figure 2a is labeled component d in Figure 27b of Wood & Churchwell, whereas the weaker 2" × 1" component about 4" to the SE of d is labeled component d$_1$. We adopt the Wood & Churchwell notation for these components. Wood & Churchwell classified component d as a member of the cometary morphological class of H II regions. Component d$_1$ was classified as a spherical region by Wood & Churchwell.

A contour plot of the 1.3 cm continuum emission in the W51 d region is shown in Figure 2b. As with the 3.6 cm data, the lack of short u, v spacings results in an insensitivity to large continuum structures. The 1.3 cm data do not reasonably image any continuum structures larger than about 1".5. Only two continuum components are seen in Figure 2b, the weaker being the edge of the W51 d H II region, which is seen as a broken arc of emission. The strongest source is a pointlike continuum region at the position of the $(J, K) = (9, 8)$ NH$_3$ masers. Extending the notation of Wood & Churchwell (1989),
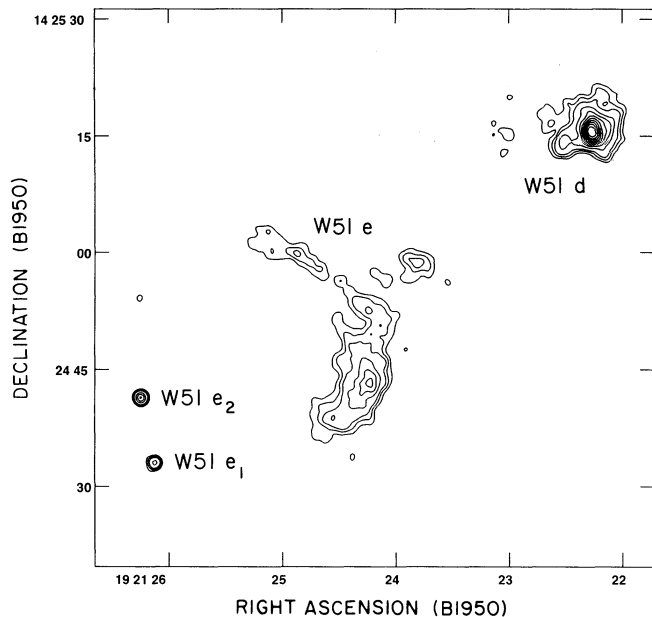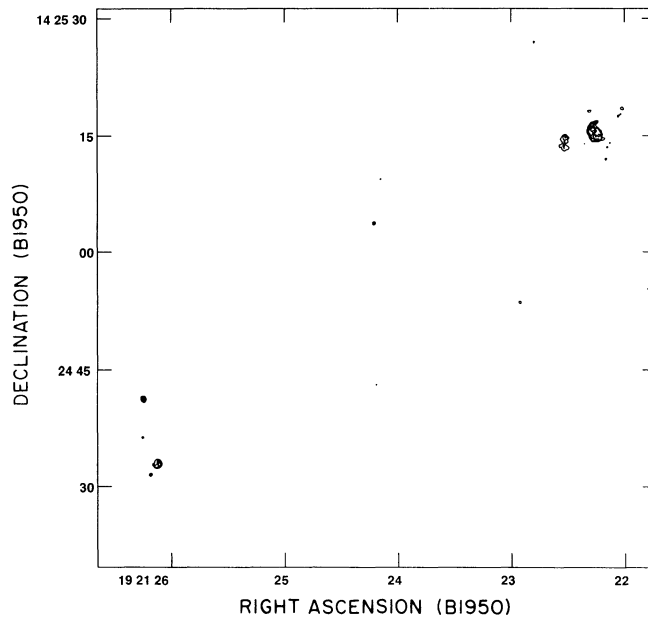
FIG. 1.—(a) 2 cm wavelength contour plot of the W51 d and e region from Gaume & Mutel (1987). The FWHM beamsize is 1″2, and the contour levels are 3%, 6%, 10%, 20%, ..., 90% of the peak flux density of 373 mJy per beam. (b) A 3.6 cm wavelength contour plot of the W51 d and e region with a FWHM beamsize of 0″27. The contour levels are 10%, 20%, ..., 90% of the peak flux density of 27 mJy per beam.

we label this continuum component d_2. This region is also seen in the 3.6 cm contour plot in Figure 2a, embedded in more extended emission. This component was first detected by Wilson et al. (1991). A Gaussian fit to the component is consistent with a beam deconvolved size of less than 0″04. This is equivalent to a linear extent of less than 300 AU. The flux density of d_2 at 3.6 and 1.3 cm (see Table 1) is consistent with that of an optically thick (at 1.3 cm) H II region.

Figures 3a, 3b, and 3c are contour plots of the W51 d region. Figure 3a is from the 2 cm image of Gaume & Mutel (1987), which, in addition to the W51 d and d_1 components, shows significant extended emission. Figure 3b is contoured from the 3.6 cm image, where much of the extended emission surrounding W51 d and d_1 is resolved out. As discussed above, incomplete sampling of the extended emission causes positive and negative errors in the 3.6 cm image shown in Figure 3b. To minimize these errors, the short u, v spacings, where the most significant errors originate, can be filtered from the data, at the cost of sensitivity. The result of such filtering is seen in Figure 3c, where spacings shorter than 150 kλ have been removed (19% of the data). The W51 d H II region, seen as an arclike source in Figure 3a, now has the appearance of a broken, or distorted shell of emission. The NW portion of the shell rim is

only apparent when both the image errors and the bright extended emission are removed through the filtering of the short spacings in the u, v plane.

Wilson et al. (1991) found the $(J, K) = (9, 8)$ NH$_3$ maser emission projected NW of continuum component d_2. Our result is consistent with their lower spatial resolution data. A Gaussian fitted position of the peak NH$_3$ maser line channel is $\alpha(1950) = 19^h21^m22^s1666 \; \delta(1950) = 14°25'11″980$. This is 0″05 NE of the Gaussian fitted position of d_2. There is a 0″003 scatter in the fitted positions of the strongest NH$_3$ maser line channels. This scatter is within the channel-to-channel measurement uncertainty of the 0″07 beam. There is no systematic trend in the fitted positions of the channel features as a function of velocity. A Gaussian fit to the data is consistent with a beam deconvolved size of less than 0″04. This implies a minimum Rayleigh-Jeans brightness temperature of 2.7×10^6 K for the maser. Within measurement errors, a single-component Gaussian fit to the velocity spectrum of the NH$_3$ maser emission produces a peak flux density (1.3 Jy), line width (0.35 km s^{-1}), and central velocity (55.3 km s^{-1}) consistent with those reported by Wilson et al. (1991).

The W51 e region is seen as a large arclike source with an extent of almost 30″ (Fig. 1a). As previously discussed, our 3.6

TABLE 1

COMPACT SOURCES

| REGION	$\alpha(1950)$	$\delta(1950)$	S (mJy)		PROJECTED DIAMETER		N_e	EM	$M_\odot$	N_i	SPECTRAL TYPE	$\dot{M}_\odot$
			3.6 cm	1.3 cm	mas	AU						
d_2	$19^h21^m22^s169$	$14°25'11″94$	2.5	19	<40	<300	1.7×10^6	5.9×10^9	1.8×10^{-4}	3.5×10^{46}	B0.5	25×10^{-6}
e_5	19 21 24.210	14 25 03.67	12	29	130×96	910×670	4.6×10^5	1.2×10^9	1.0×10^{-3}	5.4×10^{46}	B0.5	34×10^{-6}
e_1	19 21 26.127	14 24 33.00	88	<20	1500	10500	1.5×10^4	1.8×10^7	8.3×10^{-2}	1.5×10^{47}	B0	...
e_2	19 21 26.247	14 24 41.33	67	300	400×250	2800×1750	3.0×10^5	1.5×10^9	1.6×10^{-2}	5.6×10^{47}	B0	195×10^{-6}
e_3	19 21 26.179	14 24 31.51	6	<20	230	1610	6.7×10^4	5.1×10^7	1.3×10^{-3}	1.0×10^{46}	B0.5	16.4×10^{-6}
e_4	19 21 26.249	14 24 36.30	4	<20	140	980	1.1×10^5	9.2×10^7	1.3×10^{-3}	6.7×10^{45}	B0.5	12.1×10^{-6}
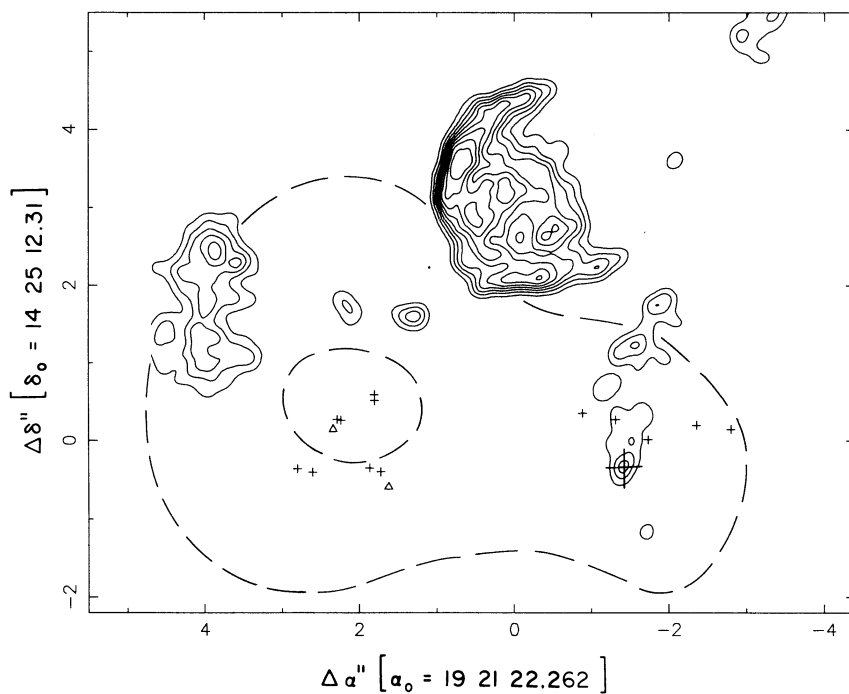
Fig. 2a
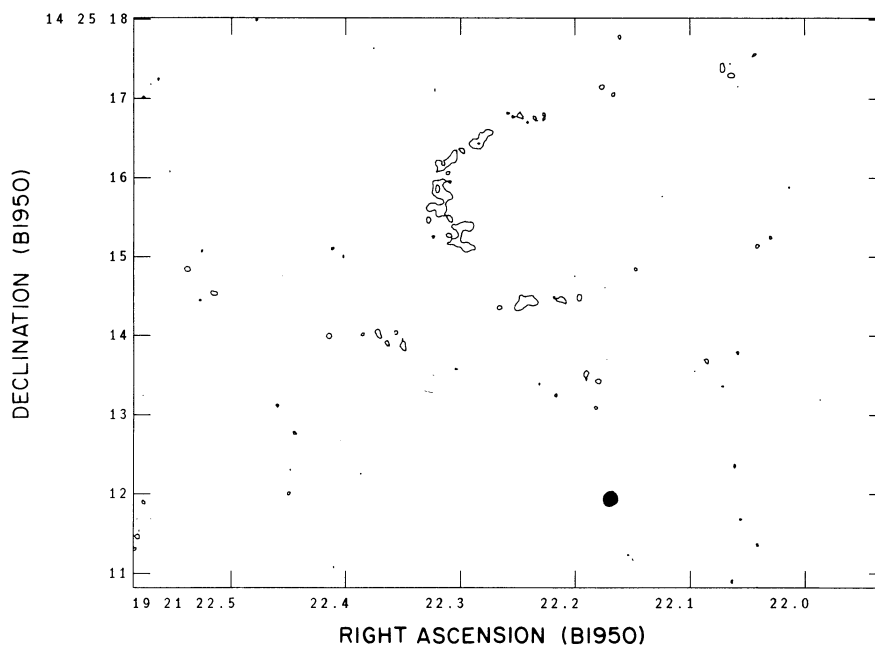

Fig. 2b

FIG. 2.—A 3.6 cm wavelength contour plot of the W51 d region with a FWHM beamsize of 0."21. The contour levels of the continuum emission are shown as solid contours and are 10%, 20%, ..., 90% of the peak flux density of 10 mJy beam^{-1}. Small crosses mark the positions of H_2O masers (Schneps et al. 1981), triangles the positions of OH masers (Gaume & Mutel 1987), a large cross the position of $(J, K) = (9, 8)$ NH_3 masers, and broken contours the $(J, K) = (3, 3)$ NH_3 thermal emission (Ho et al. 1983). (b) A contour plot of the 1.3 cm continuum emission toward W51 d with a FWHM beamsize of 0."09. The contour levels are 10%, 20%, ..., 90% of the peak flux density of 19 mJy per beam.
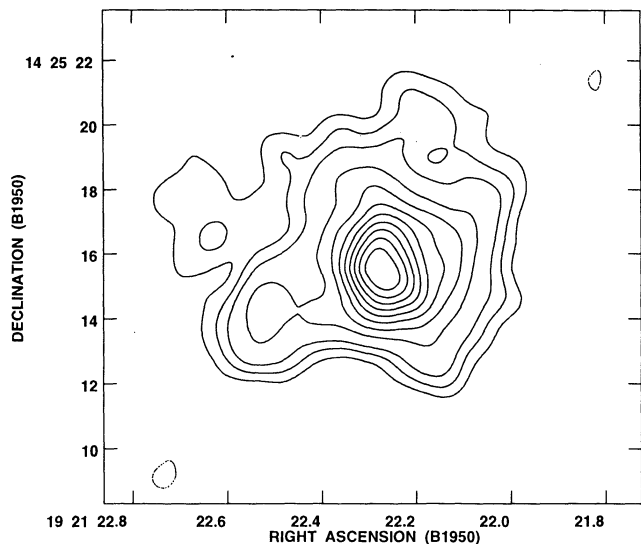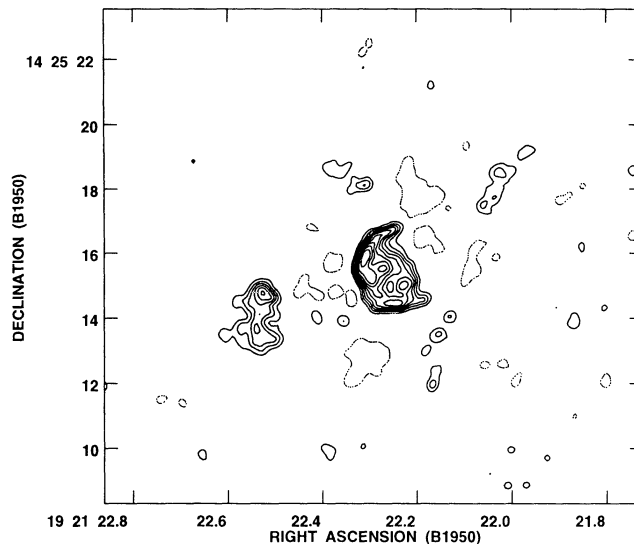
FIG. 3a

FIG. 3b
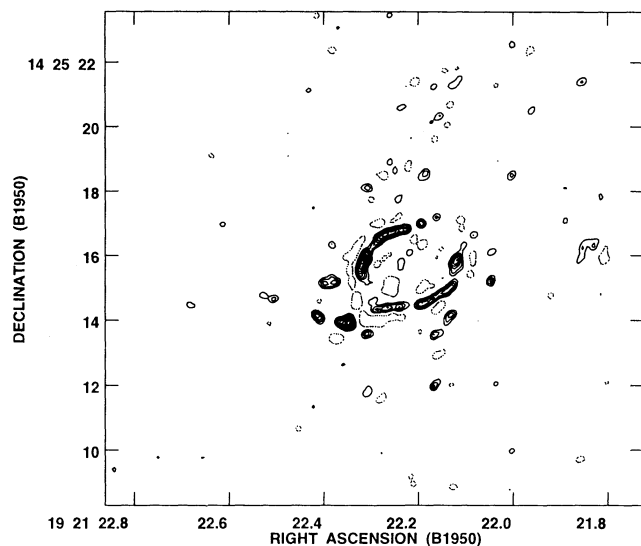

FIG. 3c

FIG. 3.—(a) 2 cm wavelength contour plot of the W51 d region from Gaume & Mutel (1987). The FWHM beamsize is 1″.2 and the contour levels are −3%, 3%, 6%, 10%, 20%, ..., 90% of the peak flux density of 373 mJy beam⁻¹. (b) A 3.6 cm wavelength contour plot of the W51 d region with a FWHM beamsize of 0″.26. The contour levels are −10%, 10%, 20%, ..., 90% of the peak flux density of 14 mJy per beam. (c) A contour plot of the 3.6 cm emission component W51 d made using a restricted data set (see § 3). The FWHM beamsize is 0″.20, and the contour levels are −15%, 15%, 25%, ..., 95% of the peak flux density of 4.4 mJy beam⁻¹.

and 1.3 cm data are biased against extended emission, and thus the W51 e region is not seen in our images. However, a previously undetected ultracompact region is imaged in our 3.6 and 1.3 cm data. This component is shown in Figures 4a and 4b. We label this region e_5. Figure 4a is a contour plot of e_5 at 3.6 cm. The triangles show the positions of 1720 MHz OH masers projected about 3″ to the NE (Gaume & Mutel 1987). Figure 4b is a contour plot of e_5 at 1.3 cm. This component is easily resolved at 1.3 cm. Single-component Gaussian fits to the 3.6 and 1.3 cm data are consistent with a deconvolved source size of 0″.13 × 0″.096, p.a. 100°. This is equivalent to a

linear size of 1050 by 700 AU (see Table 1). The spectral index of e_5 between 3.6 and 1.3 cm is consistent with an H II region with a turnover frequency near 1.3 cm.

The W51 e_1 and e_2 region is shown in Figure 5. The 3.6 cm continuum emission is shown as solid contours in Figure 5. Triangles mark the positions of OH masers (Gaume & Mutel 1987), small crosses the positions of H_2O masers (Genzel et al. 1981), a large cross the position of $(J, K) = (9, 6)$ NH_3 masers (Pratap et al. 1991), and broken contours the $(J, K) = (3, 3)$ NH_3 thermal emission (Ho et al. 1983). Several notable features are seen in Figure 5. First, two previously undiscovered continuum components have been detected. We have labeled these e_3 and e_4. Component e_3 is ≈1″.5 SE of e_1, and has a deconvolved circular size of 0″.23 (see Table 1). It is projected about 1″ NE of a water maser. Component e_4 is 4″ NE of e_1, and has a deconvolved circular size of 0″.14. The e_4 region is projected near the center of a region of NH_3 thermal emission, near OH, H_2O, and $(J, K) = (9, 6)$ NH_3 masers. The e_3 and e_4 regions were not detected at 1.3 cm. When the 1.3 cm data are corrected for primary beam attenuation at the position of the e_3 and e_4 components, the limiting flux density of these regions is less than 20 mJy beam⁻¹. This implies that these regions have a spectral index of less than 2 between 3.6 and 1.3 cm.

With the high spatial resolution of the 3.6 and 1.3 cm data, the previously known e_1 and e_2 regions are resolved. The e_1 region appears in Figure 5 to be a broken, or distorted circular shell. The SW rim of the shell is a factor of 6 brighter than to the NW. Although the integrated flux density of e_1 is significant, the peak flux density per beam is small, and thus e_1 was not detected in the lower sensitivity 1.3 cm data which has a noise level a factor of 20 worse (when corrected for primary beam response, and differing beam sizes) than the 3.6 cm data. The 1″.5 diameter of e_1 is equivalent to a linear size of 10,500 AU.

The e_2 region is the peak component (in flux density per beam) in the 3.6 cm data. Figure 6a is a contour plot of e_2 at 3.6 cm. The source is resolved, elongated in the NE-SW direction. Figure 6b is a contour plot of e_2 at 1.3 cm. With the higher resolution of the 1.3 cm data we see that the core of e_2, about 0″.2 in diameter, located near $\alpha(1950) = 19^h21^m26^s.25$ $\delta(1950) = 14°24'41''.4$, has a clumpy brightness distribution. Another
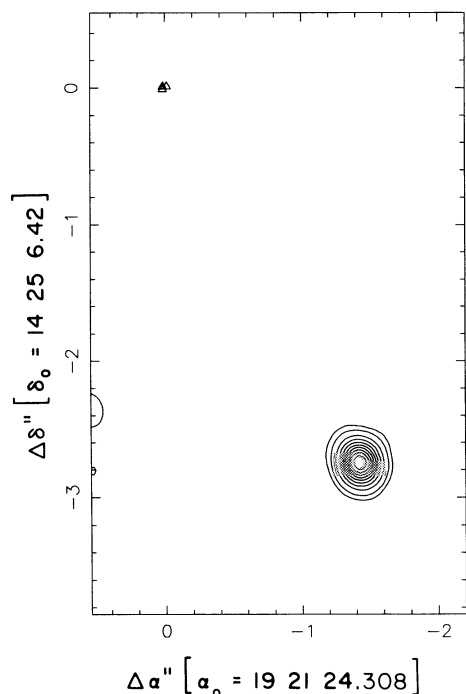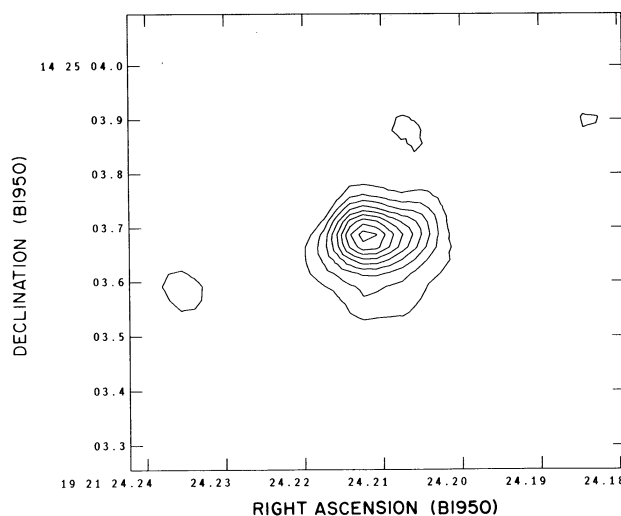
FIG. 4a

FIG. 4b

FIG. 4.—(a) A 3.6 cm wavelength contour plot of the ultracompact H II region e_5. The beamsize is 0".21 FWHM. The contour levels are 5%, 10%, 20%, ..., 90% of the peak flux density of 10 mJy beam^{-1}. The triangles show the positions of 1720 MHz OH masers projected about 3" to the NE (Gaume & Mutel 1987). (b) A 1.3 cm wavelength contour plot of the region W51 e_5 with a FWHM beamsize of 0".09. The contours are 15%, 25%, ..., 95% of the peak flux density of 13 mJy per beam.

weaker component is located about 0".2 east of the core. The extension to the SW, easily seen at 3.6 cm, is less prominent in the 1.3 cm image. When the 1.3 cm image is convolved to the same resolution as the 3.6 cm data it is evident that the SW extension and core of e_2 have different spectral indices. Figure 6c is a 3.6–1.3 cm spectral index gray-scale/contour map of the e_2 component. The spectral index in the SW extension of e_2 is ≈ 0.7 between 3.6 and 1.3 cm, whereas the spectral index in the core is ≈ 2, consistent with an optically thick H II region.

4. DISCUSSION

4.1. Cometary H II Regions

Recent surveys have attempted to classify ultracompact H II regions into one of a handful of general morphological classes. In particular, in an observation of 75 ultracompact H II regions, Wood & Churchwell (1989) identified five different morphologies: spherical or unresolved, cometary, core-halo, shell, and irregular or multiply peaked. As demonstrated by a comparison of Figures 1a with 1b, and Figures 3a with 3b and 3c, a particular ultracompact H II region can easily be mistyped or entire emission structures missed because of the observational parameters chosen for the survey. This caveat, and others concerning classification surveys, are discussed in greater detail in § IIIa of Wood & Churchwell and § 2.5 of Churchwell (1990). Although taxonomy serves a useful purpose, in this case conclusions drawn from population statistics for the various morphological classes must be viewed cautiously, at best.

One morphological type of H II region has received considerable attention of late: the cometary class. As defined by Wood & Churchwell (1989), a cometary H II region's "ionization front is parabolic and shaped like a comet. Its

leading edge is sharp and well defined. The surface brightness along the parabola's axis of symmetry decreases gradually from the head to the tail." Two H II regions with cometary shapes, Sgr B2 I and G34.3, were mapped by Benson & Johnston (1984). The cometary morphology of G34.3 was discussed by Reid & Ho (1985). Gaume & Mutel (1987) identified five cometary-shaped H II regions, including Sgr B2 I and G34.3. Of the 75 ultracompact regions mapped by their survey, Wood & Churchwell (1989) identify 15 in the cometary morphological class. Some H II regions that have been classified as cometary have extended, well-developed "tails" (e.g., G34.3+0.2, Fig. 1 Van Buren et al. 1990), whereas others are little more than bright emission arcs (e.g., G30.54+0.02, Fig. 15a of Wood & Churchwell 1989).

There has been great interest in the physical conditions which are responsible for the formation of a cometary H II region, as an identification of this mechanism may lead to a geater understanding of how a massive newly formed star interacts with the surrounding molecular cloud. To explain the cometary morphology of Sgr B2 I, Benson & Johnston (1984) proposed that component I was a stellar shell being blown away by radiation from components E, F, and G. Reid & Ho (1985) suggest that a wind from the stellar precursor to the W44 SNR is responsible for distorting the shape of G34.3 into that of a cometary H II region. Based on molecular line data, which shows hot, dense, molecular cores projected just off the front of the "upstream" side of some cometary H II regions, numerous authors have suggested a champagne flow, or a confinement of the H II region by the anisotropically distributed molecular material, as a model for the environment of cometary H II regions (e.g., Carral & Welch 1992; Fey et al. 1992; Heaton, Little, & Bishop 1989; Garay, Rodríguez, & van Gorkom 1986). The recent numerical modeling of cometary
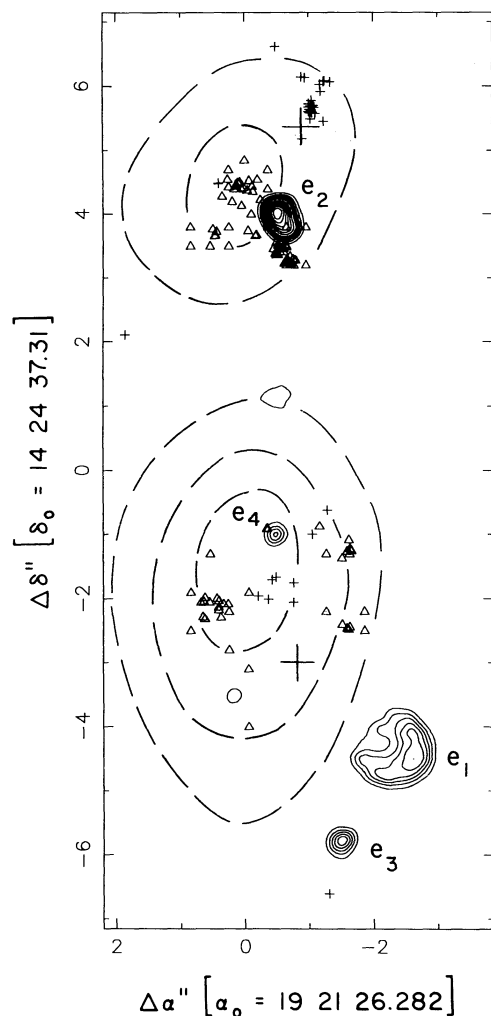
FIG. 5.—A contour plot of the 3.6 cm continuum emission toward the W51, e_1, e_2, e_3, and e_4 region shown with solid contours. The FWHM beamsize is 0".21. The contour levels are 5%, 10%, 15%, 20%, 30%, ..., 90% of the peak flux density of 20 mJy per beam. Triangles mark the positions of OH masers (Gaume & Mutel 1987), small crosses the positions of H_2O masers (Genzel et al. 1981), a large cross the position of $(J, K) = (9, 6)$ NH_3 masers (Pratap et al. 1991), and broken contours the $(J, K) = (3, 3)$ NH_3 thermal emission (Ho et al. 1983). This figure is modeled after Fig. 2 of Pratap et al. (1991).

H II regions by Van Buren et al. (1990) and Mac Low et al. (1991) suggest that cometary H II regions can be explained as a layer of ionized material created at the bow shock interface between the wind of a moving star and ambient neutral molecular material. Extending the moving-star bow shock model to all viewing angles, Mac Low et al. (1991) suggest that 85%–90% of *all* ultracompact H II regions are bow shocks. Since ram pressure confinement of the H II region greatly lengthens its lifetime, a desirable advantage of the bow shock model (see Churchwell 1990) is that the model greatly prolongs the period within which an O/B star will exhibit an observable ultracompact H II region.

Figure 2a shows the W51 d region at a wavelength of 3.6 cm. The 2" arclike H II region was classified as a cometary by Wood & Churchwell (1989). Based on the images of the region shown in Figures 2a, 3a, and 3b, we agree with this classification. Indeed, the region as seen in these contour plots closely matches the standard bow shock model for a viewing

angle of near 30° (compare with Fig. 5 of Mac Low et al. 1991). However, as discussed in § 3, filtering the short u, v spacings errors from the 3.6 cm data shows that the W51 d H II region also shares characteristics with asymmetrically bright shell sources that is, a shell whose edge exhibits an asymmetric brightness distribution (Fig. 3c). As discussed by Mac Low et al. (1991), bow shock models do not produce shells sources. Although the bow shock model appears to explain the brightest features of W51 d, the shell-like characteristics are not explained by this model. The bow shock model requires some revisions to explain acceptably W51 d. Although W51 d is only one source of many in the cometary class, the new data presented here cast some doubt on the direct application of the bow shock model to other candidate ultracompact H II regions. Additional higher sensitivity and resolution observations should be undertaken of other sources in the cometary class to determine if they too show an asymmetrically bright shell structure when observed with greater sensitivity, particularly those cometary H II regions without extended, well-developed "tails."

4.2. *Subarcsecond Ultracompact* H II *Regions*

We have imaged a number of continuum sources. We assume that these sources are ultracompact H II regions, and that they are located in the W51 d and e star formation complex. Although our observations detail a large number of H II regions in W51 d and W51 e, the W51 region does not appear to be unusual, as a large number of clustered H II regions have been detected in other regions of star formation throughout the galaxy. But, as outlined by Churchwell (1990), the existence of such a large number of standard-model, photoionized, ultracompact H II regions poses a significant problem. Driven by thermal and radiation pressures, and by stellar winds, standard-model ultracompact H II regions are believed to expand into the larger, compact H II regions (diameter $> 10^{17}$ cm) in a few 10^3–10^4 years (e.g., § 4b of Wood & Churchwell 1989). To be consistent with the large number of regions observed, either some confining mechanism must be found to prolong greatly the length of the ultracompact stage, or an upward revision in the currently favored rate of massive star formation is required.

A possible alternative explanation, for at least some ultracompact H II regions, is the notion that quasi-stable ultracompact H II regions can be formed by dense, hot, stellar winds surrounding massive stars. These stellar wind H II regions should be centrally condensed, and small. Panagia & Felli (1975) and Wright & Barlow (1975) modeled the radio emission from a spherically symmetric, infinite, constant velocity ionized wind, finding the spectral index α to be 0.6 (where $S \propto \nu^\alpha$). Others have extended the models by including recombination, acceleration, or confinement of the stellar wind (e.g., Simon et al. 1983; Reynolds 1986). These extensions to the initial stellar wind models show that the spectral index for a stellar wind H II region can vary significantly from the canonical 0.6. Stellar winds have been proposed to explain a number of ultracompact H II regions (e.g., Snell & Bally 1984).

Five continuum components with Gaussian fitted sizes of less than 1" have been detected in W51. The positions, integrated flux densities, and sizes are listed in Table 1. The equations of Mezger & Henderson (1967), as revised by Panagia & Walmsley (1978), were used to calculate electron density, emission measure, the mass of ionized hydrogen also listed in Table 1. The Lyman continuum photon flux listed in Table 1 (N_i) is
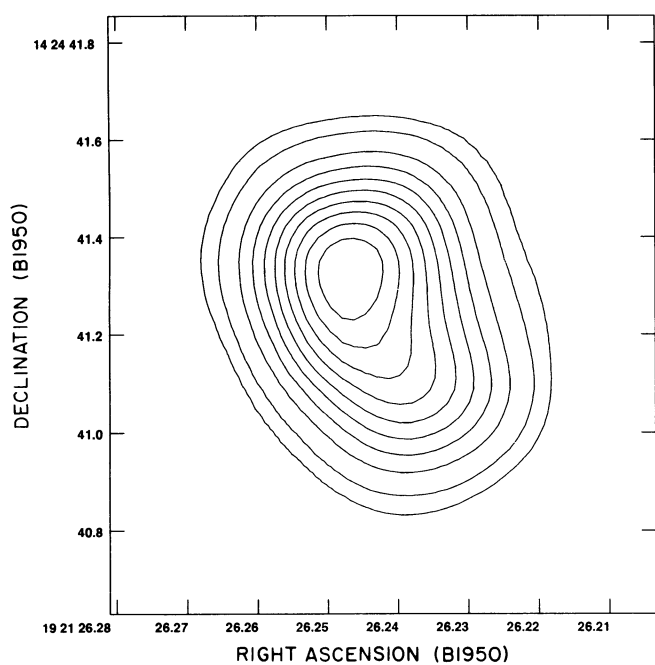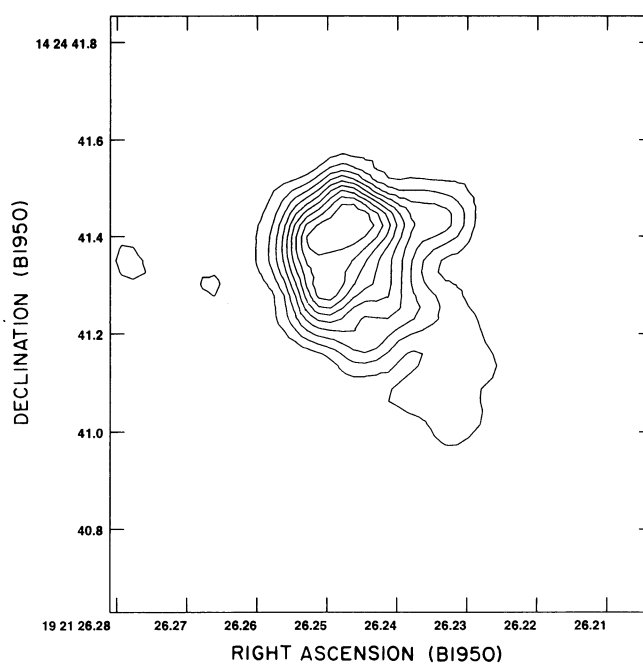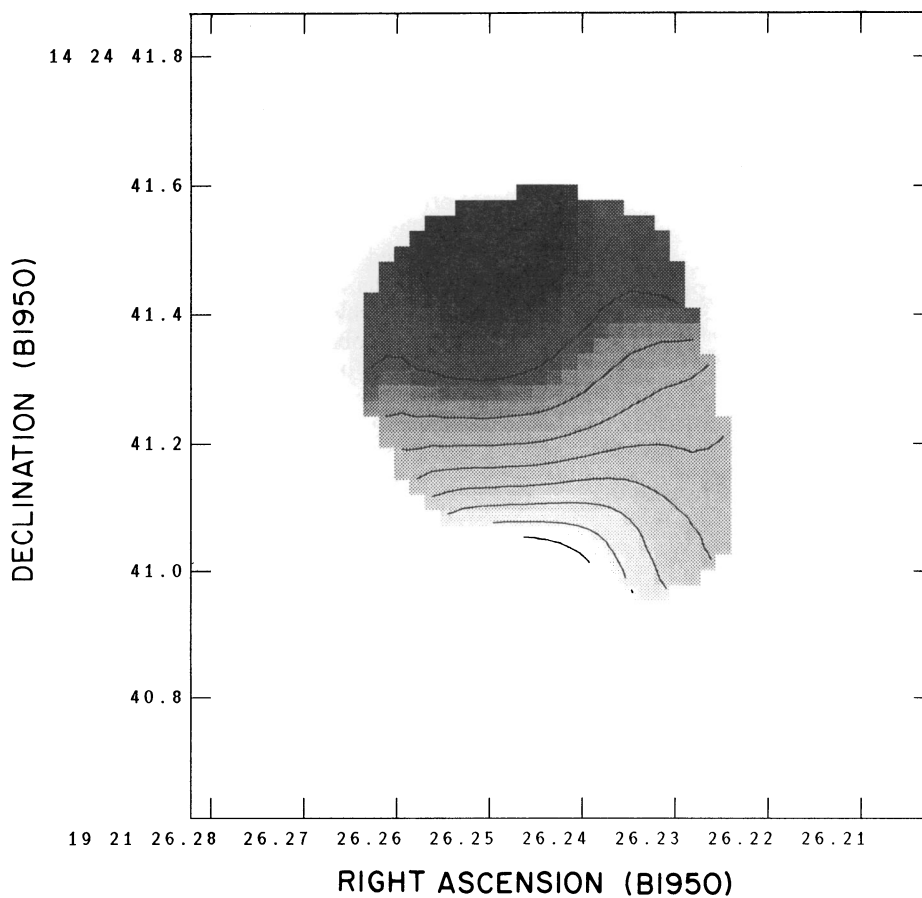
FIG. 6a

FIG. 6b

FIG. 6c

FIG. 6.—(a) Contour plot of the 3.6 cm emission from the continuum component W51 e_2 with a FWHM beamsize of 0.''21. The contour levels are 5%, 10%, 20%, ..., 90% of the peak flux density of 20 mJy per beam. (b) A 1.3 cm wavelength contour plot of the continuum emission from W51 e_2 with a FWHM beamsize of 0.''09. The contours are 10%, 20%, ..., 90% of the peak flux density of 40 mJy per beam. (c) A gray-scale plus contour overlay plot of the spectral index for W51 e_2 between 3.6 and 1.3 cm. The 10 contour lines range from 0.2 to 2.0 in spectral index in increments 0.2.

calculated using the integrated flux density. Assuming excitation by a single star allows the assignment of spectral types (Panagia 1973). The diameters of these sources range from less than 300 AU (d_2) to ≈ 3000 AU (e_2). In addition, a sixth region, W51 e_1, is slightly larger, with a projected diameter of $1''5$ (10,500 AU). With the exception of W51 e_1, which has a shell-like morphology, all of these may be stellar wind H II regions. Using the formula of Smith et al. (1987), and assuming an outflow velocity of 100 km s^{-1}, we calculate mass-loss rates listed in Table 1. The spectral index α of component e_5 is near 0.9, within measurement errors, whereas the spectral index of component d_2 is near 2.0. If both of these regions are ionized stellar winds, recombination in the wind, channeling of the flow, or acceleration of the wind is required to produce a spectral index greater than 0.6. The $(J, K) = (9, 8)$ NH$_3$ masers are projected $0''05$ (350 AU) NE of component d_2. If the actual separation between the central star of the d_2 H II region and the NH$_3$ cloud is near the projected separation, and d_2 is a dense ionized stellar wind, one must confront the problem of how a dense cloud of neutral gas can coexist with a massive ionized outflow, presumably in the process of blowing away the nearby molecular material. One possible solution is that the wind is channeled away from the NH$_3$ cloud. A more direct solution is that the central star of component d_2 has no appreciable wind, and component d_2 is a standard-model photoionized H II region. This solution is not entirely satisfactory, for unless component d_2 is extremely young, a quasi-stable mechanism must be found to confine the H II region to a diameter of less than 300 AU.

Component e_5 is 3" SW of a 1720 MHz OH maser group (see Fig. 4a), and a few arcseconds NE of the arclike compact H II region W51 e (see Fig. 1a and 1b). Given the projected separation of 3×10^{17} cm, it is unlikely that component e_5 is directly associated with the 1720 MHz OH masers. The masers are likely associated with another embedded source, identifying the e_5 region as the site of the formation of at least two massive stars.

W51 e_2 is well resolved in both the 1.3 and 3.6 cm images. Figure 6c shows a gradient in the spectral index of the e_2 component. The core of e_2 has a spectral index of ≈ 2 between 3.6 and 1.3 cm, whereas the spectral index decreases rather smoothly to the south. There are two possible explanations for this gradient in the spectral index of the e_2 component. With the current data we cannot rule out the possibility that e_2 is composed of two or more closely spaced individual components, each having a different spectral index. Alternatively, Reynolds (1986) has discussed the expected gradient in spectral index along a resolved stellar wind jet. The core of the ionized flow could exhibit an optically thick spectral index ($\alpha = 2$) with an optically thin region ($\alpha = -0.1$) farther out in the flow. Intermediate regions of the ionized flow could exhibit intermediate spectral indices. Applied to W51 e_2, this implies a one-sided collimated outflow of ionized material, as the core of the outflow (with $\alpha = 2$) would be located in the NE portion of e_2, with the ionized outflow directed to the SW. Figure 5 show the OH maser emission and $(J, K) = (3, 3)$ NH$_3$ thermal emission toward the e_2 component. The NH$_3$ thermal emission peaks about 1" to the NE of e_2, coincident with a group of 1665 and 1667 MHz OH masers found to the NE and E of e_2. A compact group of 1665, 1667, and 1720 MHz OH masers is found projected just off the southern edge of e_2. The OH maser emission covers a velocity range of 28 km s^{-1}. Spatial-velocity groupings are seen in the OH maser emission toward e_2 (see Fig. 15

of Gaume & Mutel 1987). The OH masers may originate in molecular material accelerated by the outflow. We note that no thermal or maser emission is associated with e_2 to the E (the H$_2$O masers 2" to the N are likely associated with yet another embedded source). It is possible that the NH$_3$ emission and OH masers trace a dense portion of the molecular cloud which prevents the stellar wind from flowing to the NE, resulting in the one-sided outflow to the SW.

The e_3 and e_4 regions were detected at 3.6 cm but not at 1.3 cm. This is a result of the higher noise level of the 1.3 cm data compounded with significant loss of sensitivity because of attenuation by the primary beam response of the VLA antennas. The 1.3 cm data are consistent with the spectral indices of components e_3 and e_4 being less than 2. At 1610 AU, the Gaussian fitted diameter of e_3 is 65% larger than that of e_4. Component e_3 may be associated with a H$_2$O maser (see Fig. 5). There has been some discussion about the nature of the spatial separation and possible association between the e_1 H II region and the thermal NH$_3$/OH maser complex a few arcseconds to the NE of e_1 (Benson, Mutel, & Gaume 1984; Ho et al. 1983). However, with the detection of component e_4 it appears likely that the NH$_3$, OH maser complex is heated by an embedded source, possibly component e_4 rather than by an interaction with the e_1 H II region.

The H II region W51 e_1, with a linear diameter of 1.5×10^{17} cm, is slightly larger than what normally qualifies as ultracompact. However, in practice, H II regions several times larger than e_1 commonly placed in the ultracompact class. Because of lower sensitivity and a higher noise level, e_1 was not detected at 1.3 cm, but at 3.6 cm reveals a partial shell-like structure. The observation of a shell structure suggests that e_1 is likely optically thin at 3.6 cm. W51 e_1 cannot be explained as a stellar wind, as H II regions resulting from ionized stellar winds are nominally centrally condensed. But pressure from a stellar wind does play an important role, as winds appear to be the most likely mechanism for confining the ionized gas in a shell-like H II region to the walls of the cavity (Turner & Matthews 1984).

4.3. The $(J, K) = (9, 8)$ NH$_3$ Masers

The main result in regard to the $(J, K) = (9, 8)$ NH$_3$ emission associated with W51 is a better upper limit for the size of the ammonia maser region (40 mas). This size gives a lower limit of 2.7×10^6 K for this maser. From our measurements of the brightness temperature and equation (1) of Johnston et al. (1992), it appears that this maser must be saturated, unless the beaming angle is much smaller than 0.1 sr. The saturated nature of this emission would explain the small (less than 30% over 5 years) amount of flux density variability observed. It appears that this maser may amplify the compact continuum source. Then, if the maser is saturated, the optical depth must be of order 60. Following the analysis of Wilson et al. (1991), we then estimate that the excitation temperature across the inversion doublet levels is -15 ± 8 K. This gives rise to an overpopulation in the upper doublet level of 8%. It is of interest to compare the situation for the (9, 8) maser, from para-ammonia, with that for the (9, 6) maser from ortho-ammonia, as measured by Pratap et al. (1991). The (9, 6) maser has a peak brightness temperature of more than 10^{12} K, is highly time variable, and arises from a region of less than 0.1 mas. Thus, the peak main beam brightness temperature of the (9, 8) NH$_3$ line is about 10^6 times lower, and the time variability is less than 30% over a period of more than 5 years.

With the exception of NGC 7538 (Gaume et al. 1991), ammonia masers arise only from nonmetastable ($J > K$) levels. The nonmetastable levels are populated by a combination of IR radiation or collisions, or both. Details of the excitation of nonmetastable NH_3 masers are not clear. From observations, the ortho-ammonia masers show a higher degree of time variability than para-NH_3 masers in W51. From this observation it would seem that there is an intrinsic difference between masers in ortho and para-NH_3. If so, the maser excitation process must be intrinsic to the NH_3, and *not* the result of an overlap with lines from other molecules. As stated often, however, a method has not been found thus far to invert only a few selected nonmetastable levels of NH_3 (see, e.g., Schilke 1989; Brown & Clagg 1991; Wilson & Schilke 1992).

5. CONCLUSIONS

The W51 d and e regions have been mapped at wavelengths of 3.6 and 1.3 cm wavelengths with high sensitivity and resolution resulting in the discovery of three new ultracompact H II regions. A total of five ultracompact H II regions with diameters less than 3000 AU are found in W51 d and e, leading to the possibility that there is a lengthy stellar wind phase in the evolution of massive stars which results in observable ultracompact H II regions.

The morphological classification of H II regions is severely affected by spatial sampling in interferometric measurements. The H II region W51 d, previously classified as cometary is seen to also have the properties of a shell-like H II region. The moving star bow shock model has been proposed to explain the morphology of cometary H II regions. As this model cannot produce shell sources, a revision is required to fully explain the nature of W51 d.

A new lower limit to the brightness temperature of the $(J, K) = (9, 8)$ NH_3 masers has been established as 2.7×10^6 K. These masers are probably saturated.

REFERENCES

Benson, J., & Johnston, K. 1984, ApJ, 277, 181
Benson, J., Mutel, R., & Gaume, R. 1984, AJ, 89, 1391
Brown, R. D., & Clagg, D. M. 1991, ApJ, 378, 445
Carral, P., & Welch, W. 1992, ApJ, 385, 244
Churchwell, E. 1990, A&A Rev., 2, 79
Fey, A., Claussen, M., Gaume, R., Nedoluha, G., & Johnston, K. 1992, AJ, 103, 234
Garay, G., Rodríguez, L., & van Gorkom, J. 1986, ApJ, 309, 553
Gaume, R., Johnston, K., Nguyen, H., Wilson, T. L., Dickel, H., Goss, W., & Wright, M. 1991, ApJ, 376, 608
Gaume, R., & Mutel, R. 1987, ApJS, 65, 193
Genzel, R., et al. 1981, ApJ, 247, 1039
Heaton, B., Little, L., & Bishop, I. 1989, A&A, 213, 148
Ho, P., Genzel, R., & Das, A. 1983, ApJ, 266, 596
Johnston, K., Gaume, R., Stolovy, S., Wilson, T. L., Walmsley, M., & Menten, K. 1992, ApJ, 385, 232
Mac Low, M., Van Buren, D., Wood, D., & Churchwell, E. 1991, ApJ, 369, 395
Madden, S., Irvine, W., Matthews, H., Brown, R., & Godfrey, P. 1986, ApJ, 300, L79
Martin, A. 1972, MNRAS, 157, 31
Mauersberger, R., Henkel, C., & Wilson, T. L. 1987, A&A, 173, 352
Mezger, P. G., & Henderson, A. P. 1967, ApJ, 147, 471
Panagia, N. 1973, AJ, 78, 929
Panagia, N., & Felli, M. 1975, A&A, 39, 1

Panagia, N., & Walmsley, C. M. 1978, A&A, 70, 411
Perley, R. 1989, in Synthesis Imaging in Radio Astronomy, ed. R. Perley, F. Schwab, & A. Bridle (ASP Conf. Ser. 6), 287
Pratap, P., Menten, K., Reid. M., Moran, J., & Walmsley, C. 1991, ApJ, 373, L13
Reid, M., & Ho, P. 1985, ApJ, 288, L17
Reynolds, S. 1986, ApJ, 304, 713
Rudolph, A., Welch, W., Palmer, P., & Dubrulle, B. 1990, ApJ, 363, 528
Schilke, P. 1989, unpublished thesis, Bonn Univ.
Schneps, M., Lane, A., Downes, D., Moran, J., Genzel, R., & Reid, M. 1981, ApJ, 249, 124
Scott, P. 1978, MNRAS, 183, 435
Simon, M., Felli, M., Casar, L., Fischer, J., & Massi, M. 1983, ApJ, 266, 623
Smith, H., Fischer, J., Geballe, T., & Schwartz, P. 1987, ApJ, 316, 265
Snell, R., & Bally, J. 1984, ApJ, 303, 683
Turner, B., & Matthews, H. 1984, ApJ, 277, 164
Van Buren, D., Mac Low, M., Wood, D., & Churchwell, E. 1990, ApJ, 353, 570
Wilson, T. L., Gaume, R., & Johnston, K. 1991, A&A, 251, L7
Wilson, T. L., & Henkel, C. 1988, A&A, 206, L26
Wilson, T. L., Johnston, K., & Henkel, C. 1990, A&A, 229, L1
Wilson, T. L., & Schilke, P. 1993, in Lecture Notes in Physics 412, Astrophysical Masers, ed. A. Clegg & G. Nedoluha (Berlin: Springer), 123
Wright, A., & Barlow, M. 1975, MNRAS, 170, 41
Wood, D., & Churchwell E. 1989, ApJS, 69, 31